Mass Transport in Nanochannels

Vinh Nguyen Phan, Nam-Trung Nguyen* and Chun Yang

School of Mechanical and Aerospace Engineering, Nanyang Technological University, 50 Nanyang Avenue, Singapore, 639798

Abstract: With the advancement in ultra precision technologies and micromachining processes, the fabrication of well defined nanochannels has become feasible. Nanochannels have applications in various fields such as biomedical analysis, fuel cell, and water technologies. Understanding of characteristics of fluid transport in nanoscale is currently under research, and new insights have been gained. However, there still are a number of phenomen that have not yet been described by a complete theory. Experimental investigations provide interesting results which are unique in the nanoscale and require extensive studies to be understood. This paper aims to provide a general view on the transport phenomena in nanochannels from the different aspects of theory, experiment, fabrication and simulation. The major results of this field in the recent years are also highlighted. This review contributes to the preliminary understanding of the emerging research fields of nanofluidics.

Keywords: Nanofluidics, nanochannels, capillarity, evaporation, electro viscous.

1. INTRODUCTION

Although the theoretical fundamentals of fluid mechanics at nanoscale, are typically in the range of 1 to100 nm, they have been developed in the beginning of 19th century [1], its applications only emerge as popular research fields in the recent years. The current interest in nanoscale transport phenomena is partially caused by advances in micro/nanotechnologies, which make the fabrication of devices with nanoscale precision possible. New ultra precision technologies such as ion-beam lithography and micromachining processes such as photolithography or Reactive Ion Etching (RIE) allow the fabrication of channels with at least one dimension below 100 nm. These channels are termed in this paper as nanochannels. These new nanostructures find applications in various fields such as biomedical analysis, fuel cell, and water purification. Due to the lack of fundamental knowledge on transport effects in nanochannels, the development and implementation of these applications requires an in-depth research in nanoscale fluid mechanics. Therefore, transport phenomena in nanochannel are important current research topics. The research field investigating the characteristics of fluids that are confined in structures of nanoscale and their manipulation are called nanofluidics. This paper aims to provide an overview on the transport phenomena in nanochannels from the different aspects of theory, experiment, fabrication and simulation. The major results of this field from the recent years are also highlighted. This review contributes to the preliminary understanding of the emerging research field of nanofluidics.

2. THEORY

As the characteristic length reduces to the scale of several nanometers, the mass transport is governed by unique characteristics. Firstly, due to the small scale involved, the Reynolds number is far below unity and laminar flow regime governs. Secondly, the high Knudsen number indicates that molecular flow regime that could exit for gases in nanochannels. Thirdly, the area to volume ratio increases, so effects related to surface such as surface tension, absorption, evaporation, condensation or Electric Double Layer (EDL) becomes dominant.

Continuum Assumption

Most equations which are usually used in fluid mechanics are established with continuum assumption, in which the fluid is considered to be a continuum medium rather than a discrete collection of molecules. Knudsen number is used to judge the validity of the continuum assumption. Knudsen number is the ratio between mean free path of the fluid particle to the characteristic size of the structure. For liquid, the interaction length is used instead of the mean free path.

$$\mathrm{Kn} = \frac{l}{L} \tag{1}$$

where l is the mean-free path or interaction length and L is the characteristic length of the structure. In nanochannels, L is the smallest dimension of the channels. The fluid is considered to be continuum when Knudsen number is less than 10^{-1} [2]. This condition is generally valid for the larger channels such as microchannels. However, in nanochannels, where the characteristic size shrinks down to nanoscale, the continuum assumption may no longer be valid and is an interesting topic for the research community. The general research approach is to compare the results from classical equations using continuum assumption with numerical simulation using statistical or discrete models such as molecular dynamics (MD) or Monte-Carlo method. These works explored the limit of continuum assumption. The increasing computational capacity of modern computer helps us to improve the effectiveness of such studies. Succi *et al.* [3] suggested that the difference between simulation results using MD or Lattice Boltzmann (LB) methods and analytical results using classical Navier-Stokes (NS) equations are small. Qiao and Aluru showed in their simulation study that the continuum assumption is still valid for electroosmosis flow in channels as small as 2.2 nm [4]. Generally, the interac-

*Address correspondence to this author at the School of Mechanical and Aerospace Engineering, Nanyang Technological University, 50 Nanyang Avenue, Singapore, 639798; Tel: (+65) 67904457; Fax: (+65) 67911859; E-mail: mntnguyen@ntu.edu.sg

1876-4029/10 $55.00+.00

tional length of most liquids is in the order of few nanometers. Thus, even in nanochannels with a height from tens to several hundreds of nanometers, the continuum assumption is still valid.

Flow Governing Physics

As long as the continuum assumption is still valid, the flow in nanochannels is governed by NS equation. For a incompressible fluid, the NS equation is so evaluated as:

$$\rho\left(\frac{\partial v}{\partial t}+v\cdot\nabla v\right)=-\nabla p+\mu\nabla^2 v+f \tag{2}$$

where ρ is the mass density of the fluid, v is the velocity vector, p is the pressure, μ is the dynamic viscosity and f is the other body force per volume that acts on the liquid. The Reynolds number

$$\mathrm{Re}=\frac{\rho vL}{\mu} \tag{3}$$

compares the inertial force to the viscous force and determines if the flow is laminar or turbulent. Typically, when the Reynolds number is lower than 2300, the flow is considered laminar; a Reynolds number between 2300 and 4000 indicates the transition regime while a Reynolds number is higher than 4000 and gives a turbulent flow, this assumption is also applicable for microscale channels [5]. In nanochannels, the characteristic length L is in the nanoscale. Therefore, the Reynolds number is small and usually far below unity. The flow in nanochannels is therefore laminar, which is relatively simple to be solved analytically. However, not all assumptions which are usually used an a large scale are still applicable in nanoscale. In fluid mechanics at a larger scale, non-slip boundary conditions are usually assumed. That means the velocity of the fluid next to the solid boundary is assumed to be equal to that of the boundary. However, in nanoscale, there are evidences showing that the slippage is considerable under certain conditions [6-7]. In addition, forces which are usually negligible on large scale become more important in nanoscale. The electric force acting on the Electric Double Layer (EDL) is widely used in nanoscale to drive particles using electrophoresis or to drive the flow in itself using electroosmosis. The electric force also affects the pressure driven and surface tension driven flows.

Effect of Electric Double Layer

As the characteristic length in nanochannels is comparable to the Debye length, electrokinetic effects become apparent, leading to a phenomena such as electrophoresis and electroosmosis. These phenomena is widely used in many microfluidic devices for transport and separation. The electrokinetic properties of a fluid are caused by the formation of the EDL. At the interface of the fluid and another medium, non-electrical affinities such as chemical affinity, absorption, and defect in crystal structure cause ions to attach to the surface [8]. This process is highly selective, so only certain types of ions can attach to the surface better than the others. This process makes the surface gain an electric potential which is different from the potential of the bulk fluid. The potential at the shear plane is called zeta potential. The difference in electric potential between the solid surface and the bulk fluid creates an electric field, and hence, causes ions in the fluid to redistribute. The redistribution of ions in the fluid is governed by Coulomb's Law and Poisson–Boltzmann (PB) equation. Because the electric charge density at any point in the fluid is generally not zero, the fluid responses to an external electric field.

The movement of a fluid under an applied external electric field is called electroosmosis, while the movement of small particles submerged in the fluid under an applied external electric field is called electrophoresis. The zeta potential depends on the solid material and fluid composition. There are evidences that the zeta potential be controlled by traverse external electric field [9]. The zeta potential also depends on other environmental conditions such as the formation of bubbles [10]. According to Anfken and Weber [11], the static electric charge of the surface attracts ions with opposite signs. An ion layer accumulating near the surface creates the so-called electric double layer (EDL). The EDL can be described by the distribution of electric charge density, especially at the zone near to the surface. Such density profile is governed by Coulomb's Law and Poisson-Boltzmann's Law on distribution of energy level. For a binary electrolyte $z_+ : z_-$, the PB equation reads:

$$\nabla^2\tilde{\psi}=-\frac{\rho_q e}{\varepsilon\varepsilon_0 kT}=-\frac{e^2}{\varepsilon\varepsilon_0 kT}\left[n_+^0 z_+ \exp\left(-z_+\tilde{\psi}\right)+n_-^0 z_- \exp\left(-z_-\tilde{\psi}\right)\right] \tag{4}$$

$$\rho_{\mathrm{q}}=-\varepsilon\varepsilon_0\nabla^2\psi \tag{5}$$

where ψ is the electrostatic potential, ρ_q is the charge density, e is the elementary charge, $1.6021\times10^{-19}C$, ε is the relative permittivity of the fluid, ε_0 is the permittivity of vacuum, $8.854\times10^{-12}CV^{-1}m^{-1}$, z_+ and z_- are the charge numbers, n_+^0 and n_-^0 are the bulk concentrations of cations and anions respectively, k is the Boltzmann's constant, $1.305\times10^{-23}Jmol^{-1}K^{-1}$, T is the environmental temperature, and $\tilde{\psi}=\psi e/kT$ is the normalized electrostatic potential. Based on the equations (4) and (5), the Debye thickness $\kappa^{-1}=\sqrt{\varepsilon\varepsilon_0 kT/e^2\left(z_+^2 n_+^0+z_-^2 n_-^0\right)}$ is usually used to represent the thickness of the EDL, although there were arguments that the Debye thickness does not represent well the thickness of the EDL [12]. The set of equations (4) and (5) is non-linear, so it does not have a general analytical solution. However, for a single flat wall submerged in an infinite fluid solution, the analytic solution can be found for both symmetric $z_+=-z_-$ and asymmetric $z_+\neq-z_-$ binary electrolytes [13-15]. The boundary condition in that case is $\psi=\zeta$ at the shear plane (near to the wall surface) and towards zero at infinity. For a more complicated geometry, it is much more difficult to get an analytical solution, especially for asym-

metric electrolytes. In such cases, alternative solutions can be considered. Firstly, numerical solution can be achieved. By discretizing the solution domain, the differential equation can be transformed into a system of algebraic equations and then solved numerically. This method can give useful results and the accuracy can be determined in advance, but the requirement for computing capacity is quite high for complicated geometry. Fig. (**1**) demonstrates the concepts of zeta potential and Debye length using electric potential distribution in the case of single flat wall.

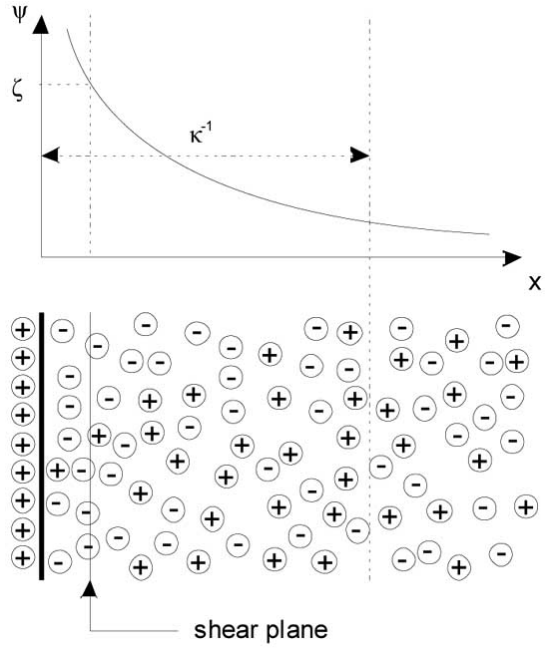

Fig. (1). Ion distribution and electric potential distribution in the case of single flat wall with positive zeta potential.

Another approach is to get the approximation for an analytical solution. For low electric potential (typically $\psi \le \zeta \le 26mV$) it is suitable to apply the linear approximation $sinh\,\tilde{\psi} \approx \tilde{\psi}$, so that the equation system can be linearized and it becomes analytically solvable for any geometry. However, the low potential approximation has limited practical applications because many solid/electrolyte pairs have higher zeta potential. For a parallel slit shaped channel, the symmetry condition $\nabla\psi|_{center} = 0$ can be applied. The analytical solution for this case was expressed in terms of elliptic function [16-17].

Using the low-potential approximation, the solution of PB equation for a slit shaped channel with boundary condition $\tilde{\psi} = \tilde{\zeta} = \dfrac{\zeta e}{kT}$ at the wall surface and $\nabla\tilde{\psi} = 0$ at the centerline, with $\tilde{\psi}$ is the normalized zeta potential, is [15]

$$\tilde{\psi}(y) = \tilde{\zeta}\frac{cosh[-\kappa y]}{cosh\left[\dfrac{\kappa h}{2}\right]} \tag{6}$$

The electric potential distribution (6) is illustrated in Fig. (**2**) for cases from thin EDL ($\kappa h >> 1$) to overlapping EDL ($\kappa h << 1$). Rice and Whitehead [18] gave the solution for the case of a cylindrical nanochannel in term of zero order modified Bessel function

$$\tilde{\psi}(r) = \tilde{\zeta}\frac{I_0(\kappa r)}{I_0(\kappa R)} \tag{7}$$

where R is the radius of the nanochannel. The electric potential distribution (7) is illustrated in Fig. (**3**) from thin EDL ($\kappa R >> 1$) to overlap EDL ($\kappa R << 1$). Li and Yang [19] reported the solution for rectangular microchannels. Low potential approximation is valid for a very narrow channel as long as the condition $z\tilde{\psi} < 1$ is satisfied. At room temperature $T = 298K$, the low-potential approximation requires that the zeta potential is less than 26mV [15]. Petsev and Lopez [20] suggested an alternative solution for the case of an EDL thickness much smaller than the channel width. In this case, the interaction between two EDLs is considered as negligible. The final potential distribution is taken as superposition of two single wall EDL potential distributions, which can be found analytically. Thin EDL approximation was used also by Levine [21] to construct the potential distribution in a cylindrical nanochannel. In that model, the inner part of the nanochannel is divided into two regions. The first region is near to the wall (inner region), where thin

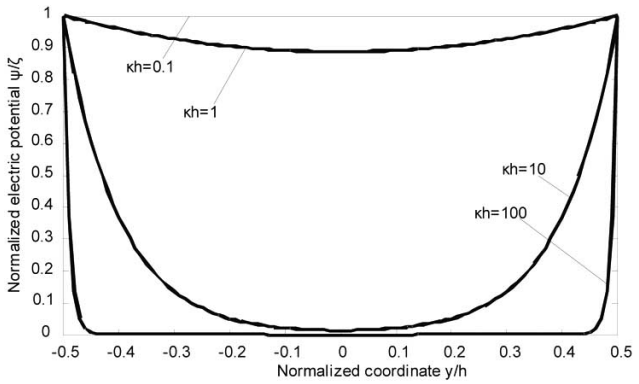

Fig. (2). Electric potential distribution in slit shaped channel with low potential approximation. The results are plotted for the cases from thin EDL ($\kappa h >> 1$) to overlap EDL ($\kappa h << 1$).

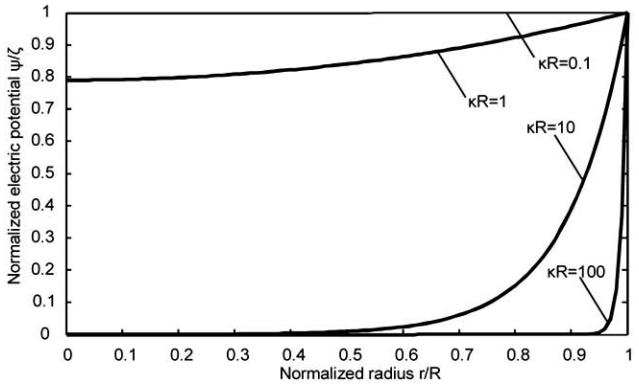

Fig. (3). Electric potential distribution in cylindrical channel with low potential approximation. The results are plotted for the cases from thin EDL ($\kappa R >> 1$) to overlap EDL ($\kappa R << 1$).

EDL approximation can be used. The second region is far away from the walls (outer region). Thin EDL approximation is not applicable here, but the potential drops are enough to justify the low-potential approximation. The solutions for these two regions are then combined by matching asymptote method to get the final distribution [20, 22, 23].

Electroosmotic Flow

The flow of electrolyte fluid in a nanochannel is described by the Navier-Stokes (NS) equation. In the case of an electrolyte in nanochannels, the NS equation reads [24, 25]

$$\mu\nabla^2 v = \nabla p + \rho_e E = \nabla p - \varepsilon\varepsilon_0\nabla^2\psi \tag{8}$$

This equation shows that the fluid can be driven by pressure or by an external electric field. As the size of the channel reduces, there are difficulties to implement pressure-driven concepts to manipulate the fluid flow. Therefore, electroosmosis is a popular method to drive a fluid in microchannels and nanochannels. Fluids can be driven simply by applying a voltage across the channel [26]. In the absence of an applied pressure, the NS equation becomes

$$\mu\nabla^2 v = \nabla p + \rho_e E = -\varepsilon\varepsilon_0\nabla^2\psi \tag{9}$$

The solution of this equation is the velocity profile of the fluid, from which other properties such as average velocity or flow rate can be determined.

Smoluchowski [27] provided the solution for electroosmotic flow in a straight channel with a uniform electric field applied along the channel. The analysis showed that the profile of the flow velocity has the same form as the profile of the electric potential. This result is valid for a constant dynamic viscosity μ and a constant electric permittivity ε [24-25]. The velocity profile is then given by

$$v(r) = -\frac{\varepsilon\varepsilon_0\zeta}{\mu}E\left[1-\frac{\psi(r)}{\zeta}\right] \tag{10}$$

From that velocity distribution, the average velocity can be obtained as:

$$U_{avg} = \frac{1}{A}\int_A v dA = -\frac{\varepsilon\varepsilon_0\zeta}{\mu}E(1-G) \tag{11}$$

Determining the average velocity U_{avg} now is equivalent to determining the coefficient *G*. The formula of *G* depends on methods used for the determination of the electric potential ψ as presented previously. If the EDL is much thinner than the smallest dimension of the channel, *G* becomes negligible [24-25, 27]. Burgreen, Nakache [28] and Hildreth [29] gave the formula of *G* for the symmetric solution in slit-shaped nanochannels in form of the integral

$$G(\zeta,\kappa h) = \frac{2}{\kappa h z\zeta}\int_{\tilde{\psi}_m}^{\tilde{\zeta}} \frac{(z\tilde{\psi})d(z\tilde{\psi})}{\sqrt{2\left[cosh(z\tilde{\psi})-cosh(z\tilde{\psi}_m)\right]}} \tag{12}$$

whose value can be determined numerically. Levine *et al*. [21] also presented an alternative formula in terms of series. The formula (12) is based on the exact solution of the electric potential profile. With the state-of-the-art computing capacity, the numerical result might not be too difficult to achieve. However, these two forms are quite challenging to use in further analysis, so various approximations were often used. Using the low-potential approximation for a slit shaped nanochannel, the formula for the *G* coefficient is

$$G = \frac{1}{h}\int_{-\frac{h}{2}}^{\frac{h}{2}} \frac{cosh(-\kappa y)}{cosh\left(\frac{\kappa h}{2}\right)}dy = \frac{2}{\kappa h}tanh\left(\frac{\kappa h}{2}\right) \tag{13}$$

This formula is quite simple and suitable for further analysis. However, (13) is only applicable for channel with zeta potential lower than 26 mV, which is less practical. Petsev [30] gave an approximation for slit shaped nanochannel with a thin EDL. This approximation is valid for an arbitrary high potential, as long as the condition $\kappa h > 4$ is satisfied. The formula of the coefficient *G* is given in terms of Lerch's transcendent, which can be easily evaluated numerically. One interesting point to raise here is that this formula is in good agreement with equation (13) in the case of low zeta potential, even for $\kappa h < 4$. Therefore, Petsev's formula has a wider use than equation (13) although it is more complicated for further analysis.

Applying low-potential approximation to a cylindrical nanochannel, coefficient *G* can be expressed by the first and zero order Bessel functions I_1, I_0 [21]:

$$G = \frac{2I_1(\kappa R)}{\kappa R I_0(\kappa R)} \tag{14}$$

where *R* is the radius of the channel. This approach has the same limitation as that of the slit shaped channel, so that it is only applicable for liquid-solid interfaces that have zeta potential less than 26 mV, which are not commonly found. Fig. (**4**) illustrates the correction coefficient *G* versus the normalized channel size for slit shaped channels and cylindrical channel. In both cases, the coefficient *G* becomes negligible when the normalized channel size reduces. On the other hand, when the normalized channel size increase, the coefficient *G* approaches 1, which suppresses the electroosmotic flow.

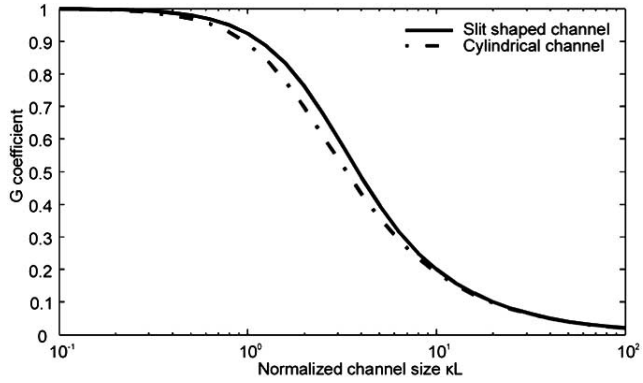

Fig. (4). Coefficient G versus the normalized channel size for slit shaped channels and cylindrical channel. L is the characteristic length of the channels, equal to the channel height for slit shaped channel and channel radius for cylindrical channel.

Petsev and Lopez [20] suggested a solution using thin-EDL approximation for a cylindrical nanochannel. The method is similar to the case of a slit shaped channel, where the space in the nanochannel is divided into inner region and outer region. The solution is assumed to depend on the radial position and the ratio κR between the radius of the nanochannel and the Debye thickness only. Under this assumption, the first order approximation is determined by the zero order Bessel function. After matching the two solutions in two regions, the final solution is

$$\tilde{\psi} = \tilde{\psi}^0 + \frac{1}{\kappa R}\tilde{\psi}^1 \tag{15}$$

Applying

$$G = \frac{1}{\zeta A}\int_A \tilde{\psi}(r)\,dA \tag{16}$$

to the case of the cylindrical nanochannel leads to:

$$G = \frac{2}{\zeta R^2}\int_0^R \tilde{\psi}(r)\,r dr = \frac{2}{\zeta R^2}\int_0^R \left[\tilde{\psi}^0(r) + \frac{1}{\kappa R}\tilde{\psi}^1(r)\right] r dr \tag{17}$$

This formula can be computed analytically although the final expression is complex. Thin-EDL approximation for micro/nanochannels provides a faster way to obtain the numerical value of *G* compared to the numerical solution of the PB equation [20]. Fig. (**5**) shows *G* coefficient versus normalized channel radius using thin-EDL approximation, with the normalized zeta potential $\tilde{\psi} = 1$. The figure shows that this approximation is not applicable for the case of thick EDL ($\kappa R < 1$) because *G* should be less than or equal to unity. However, with a thin EDL, this approximation is close to low-potential approximation, where the low-potential approximation is applicable.

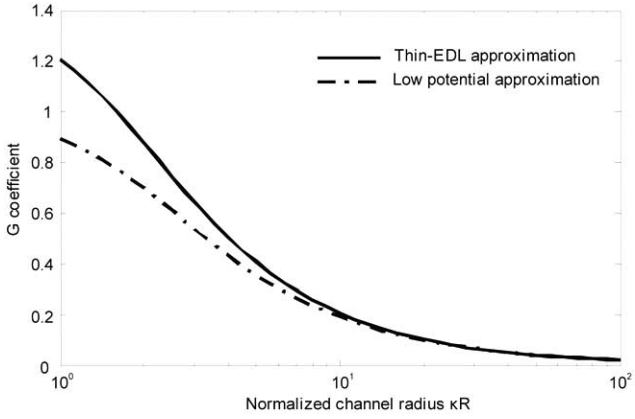

Fig. (5). Coefficient G versus the normalized channel radius for cylindrical channel using thin-EDL approximation.

Capillary Filling

The capillary filling process is traditionally described by Washburn's formula, which states the proportional relation between the filling distance and the square root of the filling time [31]. This formula is originally used to describe the capillary filling in porous material but is also applicable in channels. The capillary filling in nanochannels has been studied consistently in the recent years. Most results confirm the Washburn's model but the filling speed is usually lower than theoretically predicted. For instance, Tas *et al.* [32] filled the rectangular nanochannels with water and sodium chloride (NaCl). Han *et al*. [33] investigated the filling process using various liquids. The authors explained the reduction in filling speed by the trapping of air bubbles, which was observed during the filling process. The trapping of air was observed afterwards by other authors [34, 35].

The small size of nanochannels makes many phenomena which are usually ignored in larger channels become more important. Higher surface to volume ratio in nanoscale makes the surface effects more significant. These effects add to the complexity of the capillary filling model and causes the differences in filling behavior of a fluid in nanochannels compared to that in larger channels. Tas *et al.* [36] studied the negative pressure induced by surface tension across the water meniscus of a plug in a hydrophilic nanochannel. This negative pressure is inverted proportional to the channel height h. In a nanochannel, this negative pressure is significantly high, therefore, it can even cause deformation of the channels, as in a model suggested by Van Honschoten *et al*. [37]. The model, as shown in Fig. (**6**), indicates that the capillary filling speed in deformable nanochannels follows Washburn's law. The deformation of the nanochannels, on the one hand, increases the flow resistance, on the other hand, increases the filling driving force by increasing meniscus curvature. Mortensen and Kristensen [38] introduced a mathematical model for the electroviscous effect of capillary filling in nanochannels based on the relationship of liquid flow rate and streaming current. The theory pointed out that the apparent viscosity reaches a maximum when the characteristic channel size is comparable to the Debye thickness. However, a comparison between this theory and the experimental data from other authors [32, 34] showed that electroviscous is not sufficient to explain the overall increase in apparent viscosity. Phan *et al*. [39] proposed a analytical model by considering the formation of EDL during the filling process and reached a result with little differences from that of Mortensen and Kristensen.

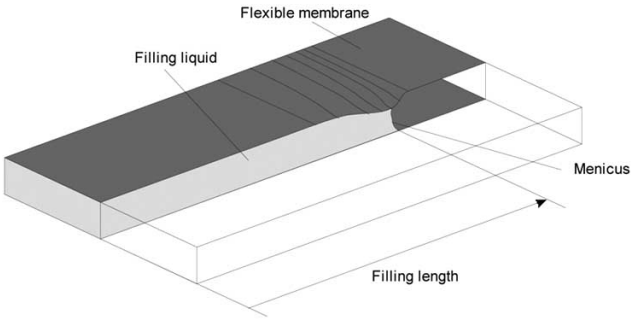

Fig. (6). Filling model presented by Van Honschoten *et al.* about elastocapillary filling in deformable nanochannels.

Although there are many efforts to figure out the phenomena that influent the capillary filling of fluid in nanochannels, a complete theory which agrees well with experi-

mental data is still under investigation. Such a theory should consider at least the electroviscous effect, the deformation of nanochannels and the formation of air bubbles. This theory, when found, will play an important roll in principle understanding as well as in application.

Electrophoretic Flow

Electrophoresis is another phenomenon of the relative motion caused by the interaction between the EDL and an external electric field. Electrophoresis process refers to the motion of suspended particle or dissolved molecules in an electric field. With the thin-EDL assumption, the fluid velocity distribution around the particle is approximately the same as electrostatic potential distribution [27]. The electrophoretic velocity is proportional to the external electric field strength:

$$U_{ep} = \frac{\varepsilon\varepsilon_0\zeta_p}{\mu E} \tag{18}$$

where ζ_p is the electrokinetic potential of the particle. In the case that the particle is much smaller than the EDL, the electrophoretic velocity is [14, 24, 25]:

$$U_{ep} = \frac{2}{3}\frac{\varepsilon\varepsilon_0\zeta_p}{\mu E} \tag{19}$$

In the case that the particle size is comparable to the EDL, the result is between the two extreme cases above. Such a problem was studied by Henry [40] and Ohshima [41].

Pressure Driven Flow

A pressure driven flow in nanochannel carries with it the electric charge associated with the EDL. The electrically charged particle movement associated with fluid flow is called the streaming current. The streaming current induces an imbalance in electric charge between two ends of the channel. The electric charge imbalance leads to a streaming potential that resists the streaming current. The streaming potential thus induces a conductive current which opposes the streaming current. This process reaches the steady state when the streaming current is equal to the conductive current [24, 25]. The process can be described by thermodynamic mean as an irreversible process [24, 42, 43]:

$$I = L_{11}\nabla\varphi + L_{12}\nabla p \tag{20}$$

$$U = L_{12}\nabla\varphi + L_{22}\nabla p \tag{21}$$

in which U is the fluid flow velocity I is the total electric current ∇P and $\nabla\varphi$ are the pressure and electric potential gradient acting along the channel. L_{ij} are the Onsager coupling coefficients. Linear assumption requires the coefficient matrix to be symmetric

$$L_{ij} = L_{ji} \tag{22}$$

In steady state, the total current vanishes, the equations (20) and (21) become

$$0 = L_{11}\nabla\varphi + L_{12}\nabla p \tag{23}$$

$$U = L_{12}\nabla\varphi + L_{22}\nabla p \tag{24}$$

The system above can be solved analytically with the elements of coefficient matrix which are determined separately [24]. The streaming potential induces a force resisting the fluid flow, on top of the viscous force. The phenomenon is called electroviscous effect. The effect is greatest for nanochannels that have characteristic dimensions equal to the EDL thickness or slightly larger. The magnitude of the viscosity increases with the zeta potential. It is estimated theoretically that the viscosity increase cannot exceed 30% for slit-shaped channels and 40% for cylindrical channels [24].

3. FABRICATION AND EXPERIMENTS

Besides the theoretical works, many works in fabrication and characterization were reported, especially in recent years. Those experiments help validate the theories and describe news observed phenomena. Advances in semiconductor processing techniques allow the fabrication of silicon-based structure in nanoscale with high accuracy. Growing, etching, bonding and surface treatment techniques with silicon-based materials are well developed. The silicon-based nanochannels are hard, therefore they are difficult to deform under external force. They are also chemically inert, hence become more reliable. It is quite easy to implement additional components on a silicon-based platform using integrated circuit fabrication techniques. Consequently, structures made of silicon-based materials are ideal for research purposes. Currently, silicon-based materials are still favored by many researchers.

Persson *et al*. [44] fabricated nanochannels in SiO_2 using double thermal oxidation scheme for their capillary filling experiments. The channel heights are from 14 to 300nm. Thamdrup *et al*. [34] also reported the fabrication of SiO_2 nanochannels with heights from 33 to 158 nm. The capillary filling experiment in these nanochannels revealed the formation of air bubbles trapping during the filling process. Van Delft *et al*. [35] embedded the nanochannels in a Fabry-Pérot interferometer. The channel heights ranged from 6 to 20 nm. The capillary filling experiments again confirmed the existence of air trapping processes. Currently, air trapping is believed to be one of the main causes of the reduction in capillary filling speed in nanochannels [33, 39]. Tas *et al*. [45] introduced a technique to fabricate silicon-based nanochannels with the heights as low as 5 nm using a thin silicon oxide spacer layer. Capillary filling experiments were carried out to test these channels. The results confirmed the reduction of filling speed by noting that the Washburn's coefficient reduces as much as 1.6 times in 5-nm-height nanochannels. The capillary filling experiments from the authors above provided important data for subsequent theoretical development, as discussed in the Theory section.

While silicon-based materials provide excellent hardness, toughness and reliability, other materials have their own ad-

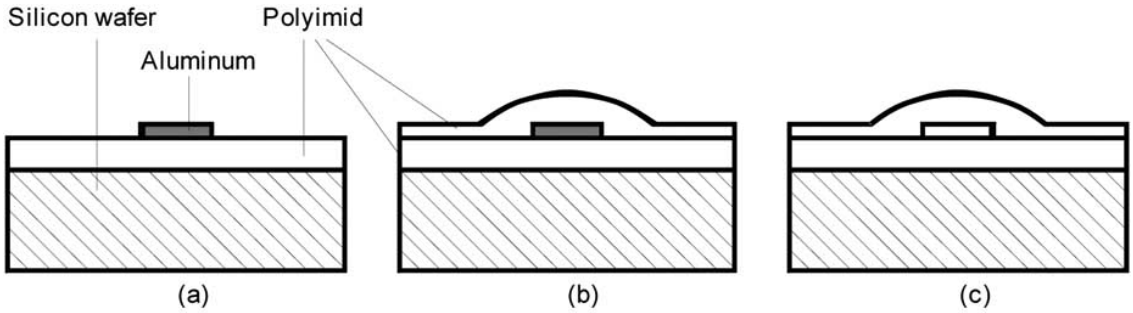

Fig. (7). Polyimid-based nanochannels fabrication principle (**a**) A layer of polyimide was spin-deposited on a silicon wafer, aluminum was deposited on top then patterned (**b**) Another layer of polyimid was spin deposited and photo patterned (**c**) Aluminum was removed by wet etching to form the nanochannel.

vantages. With low cost, variety in properties range and relatively easy to process, polymers are emerging as promising materials for fabricating nanoscale structures. Polymers provide a simpler and less expensive alternative to silicon-based materials, which is suitable for both research and mass production purpose. Recently, there are many remarkable efforts in fabrication of nanochannels using polymer, either as a major material or those that combine with silicon-based materials.

Mahabadi *et al.* [46] introduced a technique to fabricate micro and nanochannels by high-molecular-weight poly(methyl methacrylate) (PMMA) using proton beam writing and thermal bonding. Channels width was as low as 200 nm. The smoothness of the channel wall was measured to be 2.45 nm. Electroosmotic experiment was performed in these channels and was investigated by particle image velocimetry (PIV). A theoretical model was developed to predict the bulk electroosmotic flow of phosphate buffer solution in the channels. The model showed good agreement with the measured electroosmotic mobilities. Ejikel *et al.* [47] performed spontaneous filling of nanochannels with water, ethanol and isopropanol, as well as electroosmotic flow in nanochannels with heights of 100 nm and 500 nm. The nanochannels were made of polyimid, which has good electrical and mechanical properties and is biocompatible. Fabrication steps are presented in Fig. (**7**).

Jeong *et al.* [48] introduced a technique to fabricate micro and nanochannels using poly (ethylene glycol) (PEG). Plecis and Chen [49-50] described an alternative technology for the fabrication of microfluidic devices having a glass-PDMS-glass sandwich configuration. The technique uses a patterned PDMS layer as both a bonding layer and a working layer for lateral fluid confinements. The devices were tested by performing measurement of electroosmotic flows in microfluidic channels coated with different materials. The steps of fabrication are showed in Fig. (**8**).

Nichols *et al.* [58] presented sacrificially etched 2-D nanofluidic channels and nano-spaces with integrated floor and ceiling electrodes and arbitrary channel geometries. SU-8 was used as the structural materials. The channels were fabricated with channel heights ranging from 20 nmto 400 nm, channel widths from 800 nm to 40 μm, and lengths up to 3 mm.

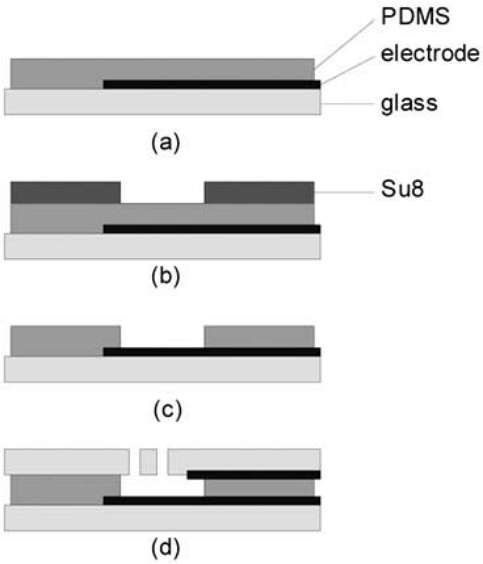

Fig. (8). Fabrication steps of PDMS-based microfluidic device proposed by Plecis and Chen [44].

The above developments in fabrication inspire many researchers to apply nanochannels in various application. Controlling, measuring properties of fluid and handling macro molecules are the common applications. Schasfoort *et al.* [9] carried out an experiment to control the magnitude and the direction of the electroosmotic flow inside a microfabricated nanochannel by applying a perpendicular electric field. The experiment introduced a microdevice called a "flowFET", which is functionality comparable to that of a field-effect transistor (FET) in microelectronics, and thus illustrating the potential of the flowFET as a controlling and switching element in microfluidic networks.

Kirby and Hasselbrink [51] presented the theory and experimental results on the zeta potential of several materials depending on cation concentration, buffer, cation type, pH, cation valency and temperature. The results showed that the Debye-Hückel approximation (low- potential approximation) can lead to serious error if being used to determine the relation between zeta potential and the counterion concentration. For silica substrate, experimental measurements showed that the high-zeta-potential limit of the PB equation is most applicable. Therefore, the zeta potential on silica substrate is

approximately proportional to the logarithm of the molar counterion concentration. The zeta potential versus pH relation was also derived experimentally by normalizing the zeta potential based on the concentration. For polymeric substrate materials, normalizing zeta potential by concentration level (pC) was suggested. Although the available data was not sufficient to obtain a complete and rigorous conclusion, it is observed that the experimental data agreed well with double layer and absorption theory.

Pu *et al*. [52] announced a new phenomenon found in nanostructures: the ion enrichment/depletion under effects of an applied voltage. The effects related to the overlapping of the EDL. A simple model was also presented to explain this phenomenon. The ion enrichment/depletion effect is demonstrated in Fig. (**9**). Sadr *et al*. [53] performed an experiment on fully developed and steady electroosmotic flow in a rectangular channel where the channel height is comparable to its width and much higher than the EDL thickness. Two components of the velocity field were measured by nanoparticle image velocimetry method. The results were within 10% of analytical prediction for mobility over a 200-fold change in concentration values.

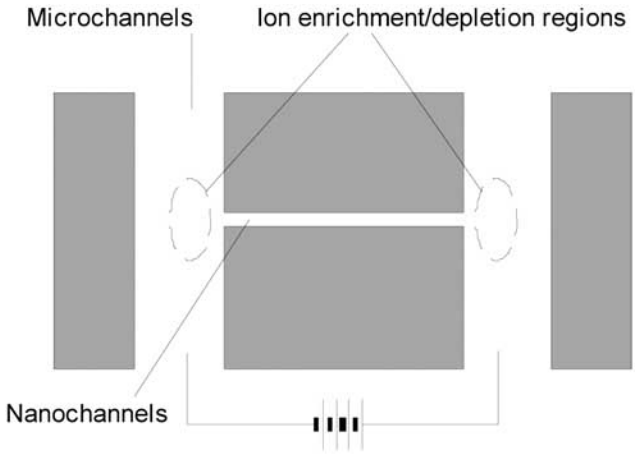

Fig. (9). The ion enrichment/depletion under effects of an applied voltage.

Mela *et al*. [54] reported the measurement of zeta potential of cyclo-olefin polymer surface as a function of pH, counter-ion concentration, storage conditions, and chemical treatment in aqueous solutions both with and without EOF-suppressing additives. Significant surface charges were measured, which contradicted the results of previous reports. The results also showed that the storage condition has relatively minor effects on the surface charge.

Van der Heyden *et al*. [55] reported measurements of the streaming current in individual rectangular silica nanochannels down to 70 nm in height. It was found that the results are best modeled using a nonlinear PB theory includes the salt-dependent hydration state of the silica surface. Firstly, streaming current is proportional to the pressure gradient and increases with the channel, height. Secondly, it is approximately constant at concentration below 10 mM, whereas it strongly decreases at higher salt concentration. And lastly, changing the sign of the surface charge reverses the streaming current. The authors also suggested applications of streaming current in energy conversion. Nath *et al*. [56] introduced a system for flow measurement in micro/nano fluidic components. The measurement was performed by arrays of straight microchannels with noncircular cross-sections. Finite difference approximation method was used to determine the flow rate. The results were confirmed in an experiment, in which the flow rates were measured by collecting the fluids on a sensitive balance while the pressure was controlled by a pump system. The investigation showed that the flow rates calculated by the finite difference approximation method were within 5.50% and 19.7% of the average experimental flow rates in the microchannels and nanochannels, respectively. Van Der Heyden *et al*. [57] carried out an experiment on the efficiency of electrical power generation in individual rectangular nanochannels by means of streaming currents. The efficiency was considered as a function of the channel height and salt concentration. It was showed that the highest efficiency occurs when the double layers overlap, which corresponds to a nanochannel, filled with solutions of low ionic strength.

Ogawa *et al*. [59] reported the fabrication of tilted and square arrays of nanopillars. Nikel plating was performed by applying a stable electric current and utilizing quartz bonding. Experiments of DNA separation with the nanopillar array showed that in the tilted array DNA showed a reptile movement. With this nanopillar array, DNA separation can be achieved. In contrast, in a square array the DNA showed a straight movement and DNA can not be separated. However, conformation change of DNA in square distribution pattern was observed. It was concluded that reptile movement is an important factor for DNA seperation. Pennathur *et al*. [60] presented an experimental study of electrokinetic transport and separation of double-stranded DNA oligonucleotides in custom-fabricated fused-silica nanochannels filled with a gel-free sodium borate aqueous buffer. The migration time of oligonucleotides depends on both the ratio of DNA molecule length to the channel depth and aspect ratio of the channel. At a background electrolyte concentrations of 1 and 5 mM, the measured electrophoretic mobility was higher than previously published values. The highest separation sensitivities were achieved in 100 nm channels with 1-10 mM ion density buffers.

Kusumaatmaja *et al*. [61] reported the effect of posts or ridges on the sides of the microchannels on capillary filling. The results showed that ridges perpendicular to the flow direction slow down filling, whereas ridges parallel to the flow may enhance filling. Hug *et al*. [62] measured electroosmotic flow of aqueous, florescent solution through the SiO_2 microchannels of 20-μm width and 4.8-μm height and nanochannels of 1-mm long and 200-nm width and height. A voltage of 10V was used to create an external electric field up to 600V/cm in the channels. Leinweber *et al*. [63] introduced the concept of continuous flow demixing of electrolytes by using structured electrode arrays. In this investigation, the axial electric potential gradient induced lateral molecular transport *via* a system of a large number of electrodes arranged orderly. A solution of electrolyte with homogeneous

concentration can be demixed to regions with different concentrations by using this method.

4. NUMERICAL INVESTIGATION AND MODELLING

Advances in computational capacity also help in developing and verifying the theories. Simulation techniques play an important role in the investigation of transport phenomena in nanochannels. Numerical models can predict the phenomena in nano- to sub nanoscale, which are difficult to perform and observe in real experiments. Changing the parameters of fluids and nanochannels is also easier in an numerical model than in experiments.

Mitchell *et al*. [64] demonstrated the simulation of electroosmotic transport in microsystems. Meshless techniques were used to find numerical solutions of the Laplace equation, the PB equation and the NS equation. The results were presented for straight channels, cross-shaped and T-shaped junctions.

Conlisk *et al*. [65] presented a model for fluid flow under the influence of an electric field in a rectangular channel. The filling fluid was a solution of a neutral sovent and a salt compound. Perfect dissociation of ions was assumed. Results showed that EDL distribution of low electrolyte concentration follows Debye-Hückel model, while at higher concentrations the distribution follows the Gouy-Chapman model. The numerical results confirmed the analytical solutions of a singular perturbation analysis. In the symmetric case, the velocity profile has the same form as the potential profile. In the asymmetric case, the two wall potentials are different, leading to discrepancies between velocity profile and potential profile. For electrically driven flow, the volumetric flow rate is proportional to the channel height. For pressure driven flow, the volumetric flow rate is proportional to the cube of the height. This result showed that for micro and nanochannels, electrokinetic pumping is a more efficient method compared to pressure driving.

Zheng *et al*. [66] described the effect of multivalent ions on electroosmotic flow. Case study with divalent ions Ca^{2+} and HPO_4^{2-} and monovalent ions K^+ and $H_2PO_4^-$ into an aqueous NaCl solution was performed. A numerical solution was derived for this case. The authors found that in micro- and nanochannels with fixed surface charges, a small amount of multivalent counterions may significantly reduce the electroosmotic flow while the multivalent co-ions do not show a noticeable effect. This effect was explained by majority of counterions in the composition of the Debye layer.

Bhattacharyya *et al*. [12] used numerical methods to analyse the electroosmotic flow in a rectangular channel with an aspect ratio on the order of unity. The condition of simulation is the same as reported by Conclisk [65]. Numerical solutions were provided for both symmetric and asymmetric velocity profile, potential and mole fraction. Results were derived for both cases with a channel height much greater than the EDL thickness and with a channel height at the same scale as the EDL thickness. It was shown that the Debye layer thickness is not a good measure of the actual width of the EDL. Results for binary electrolytes agree well with experimental data. Asymptotic solution was provided for the case of three-component mixtures. Also with the same assumption as in [65], the author reported an analysis of electroosmotic flow in a rectangular channel, where the height is much larger than the EDL thickness [67]. The results showed that at small differences of ion concentration, the Debye-Hückel approximation is appropriate. At a higher concentration difference, the Gouy-Chapman model of the EDL is more suitable. The limits of the Debye-Hückel approximation were also reported. The relationship between concentration of the electrolytes at the wall and the zeta potential was also derived. In this model, continuum assumption was adopted.

Non-equilibrium MD simulations were used by Zhu [68] to investigate the electroosmotic flow. It was found that although hydrodynamic theory is good enough to describe a simple Poiseuille flow, Poisson-Boltzmann (PB) theory shows different results from that of the simulation model. The differences were explained by the reduction in solvation of the ions. A corrected ion distribution was also introduced to keep the agreement between analytical and numerical results.

Qiao *et al*. reported a series of simulation works on the transport of ions through nanostructures [4, 69-74]. The simulations were performed with nanochannels, carbon nanotubes, and heterogeneous osmosis membranes. The results revealed some differences between simulation and theoretical approaches. A new approach for controlling turn-induced dispersion in nanofluidic channels was introduced in [70] based on the locally controlling the zeta potential at those area. The authors build an algorithm to find the optimal configuration for the zeta potential. The results showed that the dispersion can be lowered significantly. Electroosmotic flow in nanochannels with widths ranging from 0.95 to 10 nm was investigated in [69]. Both MD and continuum simulations were carried out. The simulation results for various cases showed that finite size of the ions and the discreteness of the solvent molecules affect the ion distribution in the channel significantly. In some cases, the results of MD model even showed opposite charge distribution and flow direction as that of continuum simulation. [71] The authors argued that the discrepancy is caused by the finite size of the molecules/ions and the immobilization of the ions absorbed on the channel walls, which the continuum method disregards. The scaling of electroosmotic flow and ionic conductivity in positively charged slit nanochannels were discussed in [73] using continuum and atomistic simulations. The results showed that the viscosity of the interfacial water increases substantially as the surface charge density increases and the electrophoretic mobility of the interfacial ions decreases. The effects were found to influence the scaling of the electrokinetic transport in confined nanochannels significantly. In [72], the charge distribution and velocity profile of KCl solution flows in nanochannels with different charges were analyzed using MD simulations. It was found that the counter-ion distributions are substantially different in the two

channels. Moreover, the water flux and ionic conductivity in the two channels differ by a factor of more than three. These results are not expected by continuum theory. The variations may be caused by the different sizes of the K^+ and Cl^- ions, the discreteness of the water molecules, and the asymmetric dependence of the hydrogen bonding of water near the charged silicon surface. Also using MD simulations, water and ion transport through a heterogeneous membrane separating two electrolyte solutions at different concentrations was investigated in [74]. Simulation results showed that the differential transport of K^+ and Cl^- ions through the membrane pores creates an electric potential difference across the membrane, which then induces an electroosmotic water flux.

Ramirez and Conlisk [75] carried out computational fluid dynamics (CFD) simulations of electroosmotic flow in nanochannels and examine the effects of sudden changes in channel cross-section area. The formation of vortices or recirculation regions near the step face was observed when the width of the EDL is large enough. Conlisk *et al.* [76] analysed the electroosmotic flow for both steady-state and transient two and three ionic components in a nanochannel. Numerical solution was considered. Short transient regime can be achieved by a sudden introduction of species at the inlet of the channel. Steady state electroosmotic flow was established when all important parameters such as concentration, potential, and velocity are independent of the streamwise coordinate. Direction of the movement of species is governed by the Fickian diffusion, electrophoresis phenomena and bulk convection. The results showed that in a negatively charged wall channel, the a negatively charged species may move in opposite directions of those of the bulk fluid flow. On the other hand, positively charged species are transported in the direction of fluid flow and there is significant decrease in the transit time as compared to uncharged or negatively charged species. The formulae for the concentration and species flux were derived. The comparison between steady-state model and experimental results showed a very good agreement.

Lerch and Jacobson [77] used SIMION and COMSOL to model the electric fields and fluid flow for the purpose of designing microfluidic devices with a two-dimensional planar format. The design consisted of a single channel for the first dimension which orthogonally intersected a high-aspect ratio second-dimension channel. Control channels were placed on both sides of the first-dimension channel to reduce dispersion in the second-dimension flow. Several designs were fabricated and tested. The results showed that the design with four control channels provided the most effective sample confinement. It was also showed that multiple parallel channels in the second dimension improve the performance of the device.

Zhang *et al*. [78] investigated the possibility of cavity formation due to high negative pressure across the meniscus of liquid during capillary filling process. The authors concluded that the negative pressure cannot induce the formation of cavity in nanochannels of uniform cross section. In nanochannels with non-uniform cross section, the formation may occur. However, these results are not applicable to the bubbles captured by the meniscus, which is commonly observed during capillary filling processes.

CONCLUSIONS

The basic theories on the transport in nanoscale structures have been established and continuously improved for a long time. However, due to the lack of well defined nanostructures and measurement techniques for the nanoscale, these theories are difficult to verify. Only until recent years, advances in fabrication techniques such as semiconductor manufacturing processes allow the realization of deterministic nanostructures such as nanochannels. Many experiments have been performed in these nanochannels to investigate nanoscale transport phenomena. Such experiments, on the one hand, help to verify the long-established theories, on the other hand, reveal new phenomena which have not been described before. In addition, advances in computational capacity also help in developing and verifying these theories. Simulation techniques play an important role in investigating the transport phenomena in nanochannels. Numerical models allow the prediction of new phenomena in nano- and sub nanoscale, where experiments are difficult to be carried out.

REFERENCES

[1] Reuss, F.F. In: *Sur un nouvel effet de l'electricite galvanique*, Memoires de la Societe Imperiale de Naturalistes de Moscou, Moscow, **1809**, pp. 327-337.

[2] Nguyen, N.-T. Micromixers Fundamentals, Design and Fabrication. William Andrew: New York, **2008**.

[3] Succi, S.; Mohammad, A.A.; Horbach, J. Lattice-Boltzmann simulation of dense nanoflows: A comparison with molecular dynamics and Navier-Stokes solutions. *Intl. J. Mod. Phys. C.*, **2007**, *18*(4), 667-675.

[4] Qiao, R.; Aluru, N.R. Ion concentrations and velocity profiles in nanochannel electroosmotic flows. *J. Chem. Phys.*, **2003**, *118*(10), 4692-4701.

[5] Sharp, K.V.; Adrian, R.J. Transition from laminar to turbulent flow in liquid filled microtubes. *Exp. Fluids*, **2004**, *36*(5), 741-747.

[6] Churaev, N.V.; Sobolev, V.D.; Somov, A.N. Slippage of liquids over lyophobic solid surfaces. *J. Coll. Inter. Sci.*, **1984**, *97*(2), 574-581.

[7] Eijkel, J. Liquid slip in micro- and nanofluidics: Recent research and its possible implications. *Lab on a Chip - Miniaturis. Chem. Biol.*, **2007**, *7*(3), 299-301.

[8] Lyklema, J.; van Leeuwen, H.P.; Vliet, M.; Cazabat, A.-M. *Fundament. Inter. Coll. Sci.*, Academic Press: London, **2005**.

[9] Schasfoort, R.B.M.; Schlautmann, S.; Hendrikse, J.; Van Den Berg, A. Field-effect row control for microfabricated fluidic networks. *Sci.*, **1999**, *286*(5441), 942-945.

[10] Churaev, N.V.; Ralston, J.; Sergeeva, I.P.; Sobolev, V.D. Electrokinetic properties of methylated quartz capillaries. *Adv. Coll. Inter. Sci.*, **2002**, *96*(1-3), 265-278.

[11] Arfken, G.B.; Weber, H.J. *Mathemat. Methods Physic.*, Academic Press: New York **1995**.

[12] Bhattacharyya, S.; Zheng, Z.; Conlisk, A.T. Electro-osmotic flow in two-dimensional charged micro- and nanochannels. *J. Fluid Mech.*, **2005**, *540*, 247-267.

[13] Hunter, R.J. Measuring zeta potential in concentrated industrial slurries. *Coll. Surfaces A: Physicochem. Engin. Aspects*, **2001**, *195*(1-3), 205-214.

[14] Russel, W.B.; Saville, D.A.; Schowalter, W.R. *Colloidal Dispersions*; Cambridge university press: London, **1989**.

[15] Verwey, E.J.W. Theory of the stability of lyophobic colloids. *J.Phys. Coll. Chem.*, **1947**, *51*(3), 631-636.

[16] Derjaguin, B.V.; Churaev, N.V.; Kiseleva, O.A.; Sobolev, V.D. Evaluation of the thickness of nonfreezing water films from the measurement of thermocrystallization and thermocapillary flows. *Langmuir,* **1987**, *3*(5), 631-634.

[17] Derjaguin, B.V.; Johnston, R.K. *Theory of Stability of Colloids and Thin Films*; Rice, C.l.; Wnitehead, R. Consultants Bureau: **1989**.

[18] Rice; Whitehead. Electrokinetic flow in a narrow cylindrical capillary. *J. Phys. Chem.*, **1965**, *69*, 4017-4023.

[19] Yang, C.; Li, D., Electrokinetic effects on pressure-driven liquid flows in rectangular microchannels. *J. Coll. Inter. Sci.,* **1997**, *194*(1), 95-107.

[20] Petsev, D.N.; Lopez, G.P. Electrostatic potential and electroosmotic flow in a cylindrical capillary filled with symmetric electrolyte: Analytic solutions in thin double layer approximation. *J. Coll. Inter. Sci.,* **2006**, *294*(2), 492-498.

[21] Levine, S.; Marriott, J.R.; Robinson, K. Theory of electrokinetic flow in a narrow parallel-plate channel. *J. Chem.l Soci., Faraday Transactions 2: Mol. Chem. Phys.,* **1975**, *71*, 1-11.

[22] Dyke, M.V. *Perturbation Methods in Fluid Mechanics*; Academic Press: London **1964**.

[23] Nayfeh, A.H. *Introduction to Perturbation Techniques*; Published by Wiley: **1993**.

[24] Dukhin, S.S.; Matijevic, E.; Mistetsky, A.; Derjaguin, B.V., *Surface Coll. Sci.*; USA Wiley-Insterscience **1974**.

[25] Hunter, R.J. *Zeta Potential in Colloid Science: Principles and Applications*; Academic Press: London, **1981**.

[26] Plecis, A.; Schoch, R.B.; Renaud, P. Ionic transport phenomena in nanofluidics: Experimental and theoretical study of the exclusion-enrichment effect on a chip. *Nano. Lett.*, **2005**, *5*(6), 1147-1155.

[27] Smoluchowski, Contribution a la theorie de l'endosmose electrique et de quelques phenomenes correlatifs. *Bull. Int. de l'Academie des Sciences de Cracovie,* **1903**, *8*, 182-200.

[28] Burgreen, D.; Nakache, F.R. Electrokinetic flow in ultrafine capillary slits. *J.Phys. Chem.,* **1964**, *68*(5), 1084-1091.

[29] Hildreth, D. Electrokinetic flow in fine capillary channels. *J.Phys. Chem.*, **1970**, *74*(9), 2006-2015.

[30] Petsev, D.N. Theory of transport in nanofluidic channels with moderately thin electrical double layers: Effect of the wall potential modulation on solutions of symmetric and asymmetric electrolytes. *J. Chem. Phys.*, **2005**, *123*(24), 1-12.

[31] Washburn, E.W. The dynamics of capillary flow. *Phys. Rev.*, **1921**, *17*(3), 273-283.

[32] Tas, N.R.; Haneveld, J.; Jansen, H.V.; Elwenspoek, M.; Van Den Berg, A. Capillary filling speed of water in nanochannels. *App. Phys. Lett.*, **2004**, *85*(15), 3274-3276.

[33] Han, A.; Mondin, G.; Hegelbach, N.G.; De Rooij, N.F.; Staufer, U., Filling kinetics of liquids in nanochannels as narrow as 27 nm by capillary force. *J. Coll. Inter. Sci.*, **2006**, *293*(1), 151-157.

[34] Thamdrup, L.H.; Persson, F.; Bruus, H.; Kristensen, A.; Flyvbjerg, H. Experimental investigation of bubble formation during capillary filling of Si O2 nanoslits. *Appl. Phys. Lett.,* **2007**, *91*(16), 163501-163505.

[35] Van Delft, K.M.; Eijkel, J.C.T.; Mijatovic, D.; Druzhinina, T.S.; Rathgen, H.; Tas, N.R.; Van Den Berg, A.; Mugele, F. Micromachined Fabry-Perot interferometer with embedded nanochannels for nanoscale fluid dynamics. *Nano Lett.,* **2007**, *7*(2), 345-350.

[36] Tas, N.R.; Mela, P.; Kramer, T.; Berenschot, J.W.; Van Den Berg, A. Capillarity induced negative pressure of water plugs in nanochannels. *Nano Lett.*, **2003**, *3*(11), 1537-1540.

[37] Van Honschoten, J.W.; Escalante, M.; Tas, N.R.; Jansen, H.V.; Elwenspoek, M., Elastocapillary filling of deformable nanochannels. *J. Appl. Phys.*, **2007**, *101*(9), 094310-094317.

[38] Mortensen, N.A.; Kristensen, A. Electroviscous effects in capillary filling of nanochannels. *Appl. Phys. Lett.,* **2008**, *92*(6), 063110-063113.

[39] Phan, V.N.; Yang, C.; Nguyen, N.T. Analysis of capillary filling in nanochannels with electroviscous effects. *Microfluid. Nanofluid.*, **2009**, *7*(4), 519-530.

[40] Henry, D.C. The Cataphoresis of Suspended Particles Part I The Equation of Cataphoresis. Proceedings of the Royal Society of London: London, **1931**. *133*.

[41] Ohshima, H. A simple expression for Henry's function for the retardation effect in electrophoresis of spherical colloidal particles. *J. Coll. Inter. Sci.,* **1994**, *168*(1), 269-271.

[42] De Groot, S.R.; Mazur, P. Non-equilibrium thermodynamics. *Courier Dover Publications*: New York **1984**.

[43] Onsager, L. Reciprocal relations in irreversible process. *Phys. Rev.*, **1931**, *37*, 405-426.

[44] Persson, F.; Thamdrup, L.H.; Mikkelsen, M.B.L.; Jaarlgard, S.E.; Skafte-Pedersen, P.; Bruus, H.; Kristensen, A. Double thermal oxidation scheme for the fabrication of SiO2 nanochannels. *Nanotechnology,* **2007**, *18*, 246301-246304.

[45] Tas, N.R.; Haneveld, J.; Jansen, H.V.; Elwenspoek, M.; Brunets, N. Capillary filling of sub-10 nm nanochannels. *J. Appl. Phys.,* **2008**, *104*, 014301-014309.

[46] Mahabadi, K.A.; Rodriguez, I.; Haur, S.C.; Van Kan, J.A.; Bettiol, A.A.; Watt, F. Fabrication of PMMA micro- and nanofluidic channels by proton beam writing: Electrokinetic and morphological characterization. *J. Micromech. Microengin.,* **2006**, *16*(7), 1170-1180.

[47] Eijkel, J.C.T.; Bomer, J.; Tas, N.R.; Van Den Berg, A., 1-D nanochannels fabricated in polyimide. *Lab on a Chip - Miniaturis. Chem. Biol.,* **2004**, *4*(3), 161-163.

[48] Jeong, H.E.; Kim, P.; Kwak, M.K.; Seo, C.H.; Suh, K.Y. Capillary kinetics of water in homogeneous, hydrophilic polymeric micro-To nanochannels. *Small,* **2007**, *3*(5), 778-782.

[49] Plecis, A.; Chen, Y. Fabrication of microfluidic devices based on glass-PDMS-glass technology. *Microelectron. Engin.,* **2007**, *84*(5-8), 1265-1269.

[50] Plecis, A.; Chen, Y. Improved glass-PDMS-glass device technology for accurate measurements of electro-osmotic mobilities. *Microelectron. Engin.*, **2007**.

[51] Kirby, B.J.; Hasselbrink Jr, E.F. Zeta potential of microfluidic substrates. *Electrophoresis,* **2004**, *25*(2), 187-202.

[52] Pu, Q.; Yun, J.; Temkin, H.; Liu, S. Ion-enrichment and ion-depletion effect of nanochannel structures. *Nano Lett.,* **2004**, *4*(6), 1099-1103.

[53] Sadr, R.; Yoda, M.; Zheng, Z.; Conlisk, A.T. An experimental study of electro-osmotic flow in rectangular microchannels. *J. Fluid Mech.*, **2004**, *506*, 357-367.

[54] Mela, P.; van den Berg, A.; Fintschenko, Y.; Cummings, E.B.; Simmons, B.A.; Kirby, B.J. The zeta potential of cyclo-olefin polymer microchannels and its effects on insulative(electrodeless) dielectrophoresis particle trapping devices. *Electrophor.,* **2005**, *26*(9), 1792-1799.

[55] Van Der Heyden, F.H.J.; Stein, D.; Dekker, C. Streaming currents in a single nanofluidic channel. *Phys. Rev. Lett.,* **2005**, *95*(11), 1-4.

[56] Nath, P.; Roy, S.; Conlisk, T.; Fleischman, A.J. A system for micro/nano fluidic flow diagnostics. *Biomed. Microdev.,* **2005**, *7*(3), 169-177.

[57] Van Der Heyden, F.H.J.; Bonthuis, D.J.; Stein, D.; Meyer, C.; Dekker, C. Power generation by pressure-driven transport of ions in nanofluidic channels. *Nano Lett.,* **2007**, *7*(4), 1022-1025.

[58] Nichols, K.P.; Eijkel, J.C.T.; Gardeniers, H.J.G.E. Nanochannels in SU-8 with floor and ceiling metal electrodes and integrated microchannels. *Lab on a Chip - Miniaturis. Chem. Biol.,* **2007**, *8*(1), 173-175.

[59] Ogawa, R.; Kaji, N.; Hashioka, S.; Baba, Y.; Horiike, Y. Fabrication and characterization of quartz nanopillars for DNA separation by size. *Japanese J. Appl. Phys. Part 1: Regul. Pap. Short Notes Rev. Pap.*, **2007**, *46*(4 B), 2771-2774.

[60] Pennathur, S.; Baldessari, F.; Santiago, J.G.; Kattah, M.G.; Steinman, J.B.; Utz, P.J. Free-solution oligonucleotide separation in nanoscale channels. *Analyt. Chem.,* **2007**, *79*(21), 8316-8322.

[61] Kusumaatmaja, H.; Pooley, C.M.; Girardo, S.; Pisignano, D.; Yeomans, J.M. Capillary filling in patterned channels. *Phys. Rev. E - Stat. Nonlin. Soft Matt. Phys.,* **2008**, *77*(6).

[62] Hug, T.S.; de Rooij, N.F.; Staufer, U. Fabrication and electroosmotic flow measurements in micro- and nanofluidic channels. *Microfluid. Nanofluid.*, **2006**, *2*(2), 117-124.

[63] Leinweber, F.C.; Eijkel, J.C.T.; Bomer, J.G.; Van Den Berg, A. Continuous flow microfluidic demixing of electrolytes by induced charge electrokinetics in structured electrode arrays. *Analyt. Chem.*, **2006**, *78*(5), 1425-1434.

[64] Mitchell, M.J.; Qiao, R.; Aluru, N.R. Meshless analysis of steady-state electro-osmotic transport. *J. Microelectromech. Sys.,* **2000**, *9*(4), 435-449.

[65] Conlisk, A.T.; McFerran, J.; Zheng, Z.; Hansford, D. Mass transfer and flow in electrically charged micro- and nanochannels. *Analyt. Chem.*, **2002**, *74*(9), 2139-2150.

[66] Zheng, Z.; Hansford, D.J.; Conlisk, A.T. Effect of multivalent on electroosmotic flow in micro- and nanochannels. *Electrophoresis,* **2003**, *24*(17), 3006-3017.

[67] Conlisk, A.T. The Debye-Hu?ckel approximation: Its use in describing electroosmotic flow in micro- and nanochannels. *Electrophor.,* **2005**, *26*(10), 1896-1912.

[68] Zhu, W.; Singer, S.J.; Zheng, Z.; Conlisk, A.T. Electro-osmotic flow of a model electrolyte. *Phys. Rev. E - Stat. Nonlin. Soft Matter Phys.*, **2005**, *71*(4), 041501.

[69] Qiao, R.; Aluru, N.R. A typical dependence of electroosmotic transport on surface charge in a single-wall carbon nanotube. *Nano Lett.,* **2003**, *3*(8), 1013-1017.

[70] Qiao, R.; Aluru, N.R. Dispersion control in nano-channel systems by localized ?-potential variations. *Sensors Actuators A: Phys.*, **2003**, *104*(3), 268-274.

[71] Qiao, R.; Aluru, N.R. Charge inversion and flow reversal in a nanochannel electro-osmotic flow. *Phys. Rev. Lett.,* **2004**, *92*(19), 198301-198301.

Received: July 29, 2010 Revised: November 09, 2010 Accepted: November 14, 2010

[72] Qiao, R.; Aluru, N.R. Atomistic simulation of KCl transport in charged silicon nanochannels: Interfacial effects. *Coll. Surfaces A: Physicochem. Engin. Aspects,* **2005**, *267*(1-3), 103-109.

[73] Qiao, R.; Aluru, N.R. Scaling of electrokinetic transport in nanometer channels. *Langmuir,* **2005**, *21*(19), 8972-8977.

[74] Qiao, R.; Georgiadis, J.G.; Aluru, N.R. Differential ion transport induced electroosmosis and internal recirculation in heterogeneous osmosis membranes. *Nano Lett.,* **2006**, *6*(5), 995-999.

[75] Ramirez, J.C.; Conlisk, A.T. Formation of vortices near abrupt nano-channel height changes in electro-osmotic flow of aqueous solutions. *Biomed. Microdev.,* **2006**, *8*(4), 325-330.

[76] Conlisk, A.T.; Kumar, A.; Rampersaud, A. Ionic and biomolecular transport in nanochannels. *Nanoscale and Microscale Thermophys. Engin.,* **2007**, *11*(1-2), 177-199.

[77] Lerch, M.A.; Jacobson, S.C. Electrokinetic fluid control in two-dimensional planar microfluidic devices. *Analyt. Chem.,* **2007**, *79*(19), 7485-7491.

[78] Zhang, R.; Ikoma, Y.; Motooka, T. Negative capillary-pressure-induced cavitation probability in nanochannels. *Nanotechnology,* **2010**, *21*(10), 105706.